Image Segmentation and Selective Smoothing by Using Mumford–Shah Model

Song Gao and Tien D. Bui, *Member, IEEE*

***Abstract*—Recently, Chan and Vese developed an active contour model for image segmentation and smoothing by using piecewise constant and smooth representation of an image. Tsai *et al.* also independently developed a segmentation and smoothing method similar to the Chan and Vese piecewise smooth approach. These models are active contours based on the Mumford–Shah variational approach and the level-set method. In this paper, we develop a new hierarchical method which has many advantages compared to the Chan and Vese multiphase active contour models. First, unlike previous works, the curve evolution partial differential equations (PDEs) for different level-set functions are decoupled. Each curve evolution PDE is the equation of motion of just one level-set function, and different level-set equations of motion are solved in a hierarchy. This decoupling of the motion equations of the level-set functions speeds up the segmentation process significantly. Second, because of the coupling of the curve evolution equations associated with different level-set functions, the initialization of the level sets in Chan and Vese's method is difficult to handle. In fact, different initial conditions may produce completely different results. The hierarchical method proposed in this paper can avoid the problem due to the choice of initial conditions. Third, in this paper, we use the diffusion equation for denoising. This method, therefore, can deal with very noisy images. In general, our method is fast, flexible, not sensitive to the choice of initial conditions, and produces very good results.**

***Index Terms*—Curve evolution, image segmentation and denoising, level-set methods, Mumford–Shah functional.**

I. Introduction

IMAGE segmentation and smoothing are two popular problems in image processing and computer vision. The Mumford and Shah variational model [15] is one of the most widely studied mathematical models that can achieve both goals simultaneously by using a piecewise smooth representation of an image [19], [20]. Mumford–Shah variational methods have been extensively used in image processing because of their flexibility and various advantages in numerical implementation. The basic idea of variational methods is to minimize an energy functional $F(u, C)$ that contains a boundary C and the region u of an image. If C is a closed curve, the image domain Ω is partitioned into two subdomains R and $\overline{R}$. A classical approach to solve the minimization problem is to solve the corresponding Euler–Lagrange equation, which is a second order *partial differential equation* (PDE). Variational methods have been used in many areas such as image segmentation, object tracking, texture synthesis, and vector field visualization [2].

Based on the variational method, different image segmentation approaches have been developed, such as classical snakes based on gradient [9], geodesic active contours [4], curve evolution based on the Mumford and Shah functional method [19], and active contours without edges [6], [20]. A problem related to image segmentation is the object detection problem by snakes or active contours. An initial curve evolves in an image and stops at the boundaries of objects within the image. In most of those region based models, both the image information near the evolving contour and the image statistics inside and outside the contour have been used in order to improve the performance [25], [26]. The classical active contour models [4], [9] use the gradient of the image for stopping criteria. The active contours (or snakes) stop on the boundaries where the magnitude of the gradient of the image is large. These active contour models are usually called boundary-based models. A review on those topics can be found in [2], and the applications in multimedia such as motion segmentation and tracking can be found in [8], [13].

For image smoothing, the techniques developed from PDEs have become an active field of research. Particularly the anisotropic diffusion model originally introduced by Perona and Malik [16] and further developed by [1], [5]. Other anisotropic diffusion techniques such as curve evolution methods based on geometric scale space [10]–[12], and the construction of diffusion tensors that contain the information of both the modulus and directions of the gradients [21]–[23] have also been developed. The basic idea of most anisotropic diffusion techniques is to employ the gradient (both modulus and direction) of the intensity to detect the edges between regions then smooth the image within the homogeneous region and along the edges but not across the boundaries of such regions.

Recently, Chan and Vese developed an active contour model to deal with the problem of image segmentation and smoothing by using piecewise constant representation in [6], and piecewise smooth representation in [20]. Tsai *et al.* [19] also independently developed segmentation and smoothing method very similar to the Chan and Vese piecewise smooth approach. These methods are based on the Mumford–Shah variational method and applied to solving image segmentation and smoothing problems that can be formulated by the *level-set methods* introduced by Osher and Sethian [17]. We can consider these models as *active contours based on the Mumford–Shah model with level-set methods*. The energy functional $F(u, C)$ contains a closed segmenting curve C and image data u. The region inside C is denoted by u^{I} and

Manuscript received February 2, 2003; revised September 15, 2004. This work was supported in part by research grants from the Natural Sciences and Engineering Research Council of Canada and in part by the Fond pour la Formation de Chercheurs et l'Aide à la Recherche of Quebec. The associate editor coordinating the review of this manuscript and approving it for publication was Dr. Eli Saber.

The authors are with the Department of Computer Science, Concordia University, Montreal, QC H3G 1M8 Canada (e-mail: sgao@cse.concordia.ca; bui@cse.concordia.ca).

Digital Object Identifier 10.1109/TIP.2005.852200

the outside region by u^{II}. Minimizing the energy functional F with respect to u^{I}, u^{II} and C, we can obtain the curve evolution PDE, and the optimal estimation equations for u^{I} and u^{II}. The motion of the curve is obtained by solving the curve evolution PDE. The curve stops on the edges of objects within the given image. The optimal estimation equations for u^{I} and u^{II} have a smoothing effect on the original image u_0 [20]. Therefore, u^{I} and u^{II} obtained by solving the corresponding optimal estimation PDEs are piecewise smooth approximations of u_0 inside and outside the curve C, respectively. The curve evolution PDE together with the optimal estimation PDEs produce piecewise smoothing and segmentation of an image simultaneously [19], [20], but shortcomings also exist in this approach. Because of the coupling between the curve evolution PDE and the optimal estimation PDEs for u^{I} and u^{II}, the solutions of u^{I} and u^{II} are needed for each step of the solution to the curve evolution PDE. Therefore, it involves solving the optimal estimation PDEs for u^{I} and u^{II} at each curve evolution step, and as a consequence this approach is very slow. To see the inefficiency of this approach it is noted that the segmentation of an image only finishes at the final iteration, and only the final solutions of u^{I} and u^{II} are needed in the piecewise smooth reconstruction of the image. However, all the intermediate solutions of u^{I} and u^{II} before the final step are required for solving the curve evolution PDE. Furthermore, the optimal estimation PDEs for u^{I} and u^{II} are Poisson equations, their capability of denoising is limited.

Apart from the computational costs and the low denoising capability mentioned above, handling the initial conditions correctly is another problem of this multiphase approach. As mentioned in [20], in the implementation through the level-set method with one level-set function, we can represent only two phases in an image. In order to represent images with more complicated features, multiple level-set functions should be used. Because the Mumford–Shah problems are nonconvex, and because there is no uniqueness for the minimizer, the final segmented results may depend on the choices of the initial curves. The multiple seed initialization used by Chan and Vese [20] cannot always produce good results (see Fig. 1). We will discuss the initialization problem further in Section IV.

In this paper, we propose a new algorithm for image segmentation and smoothing. Based on the Chan–Vese piecewise constant segmentation model and the level-set method, we propose a new hierarchical method of multiphase level-set framework for piecewise constant segmentation of images. Our multiphase segmentation method is divided into different stages; at each segmentation stage only one curve evolution equation (equivalent to one level-set equation) is used. The next segmentation stage begins after the previous stage has been completed. This continues until the last stage. The number of stages is the same as the number of level-set functions. This hierarchical segmentation method makes the algorithm fast and initial conditions easy to handle. We use diffusion equation for image denoising because it can deal with very noisy images. The proposed method actually works in two steps: for a given image, we first apply the hierarchy piecewise constant segmentation method to partition the image, then apply diffusion filtering to different regions independently, but not across the boundaries of such regions.

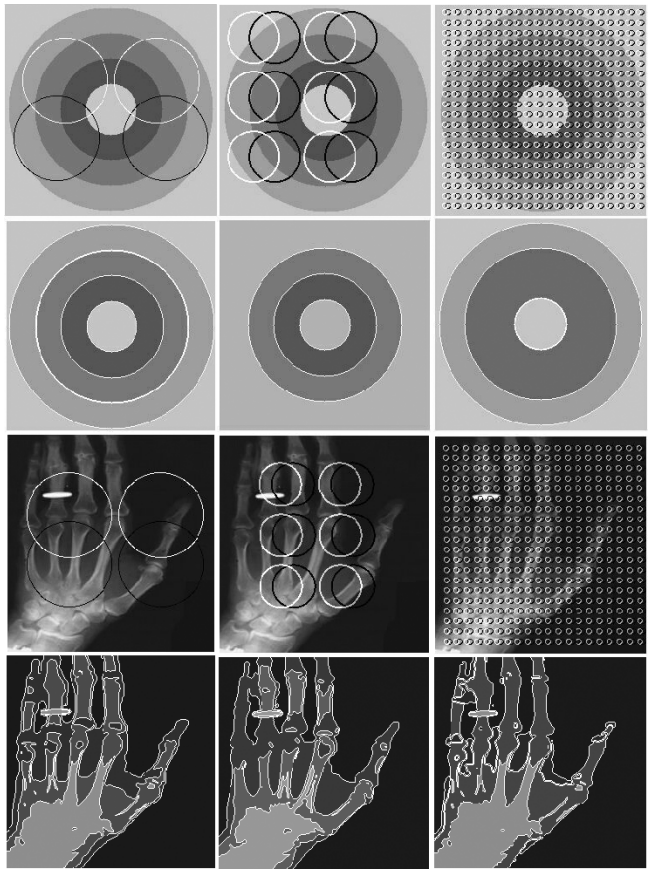

Fig. 1. Segmentation by using Chan–Vese multiphase model. The first and third rows show different initial conditions: white curves for ϕ_1 and black curves for ϕ_2. The second and fourth rows are the corresponding segmentations. Synthetic image: CPU $= 28.2$ s ($\nu = 343$). X-ray hand image: CPU $= 60.1$ s ($\nu = 431$). Image size: 256×256.

This method is fast, more flexible, and not sensitive to the initial conditions.

This paper is organized as follows. In Section II, we present different image segmentation (and smoothing) algorithms based on the concepts of the Mumford–Shah model, namely the Chan–Vese piecewise smooth active contours model [20] (also the algorithm of Tsai *et al.* [19]) for image segmentation and denoising, the piecewise constant image segmentation algorithms including the Chan–Vese level-set approach, and the direct energy computation method. In Section III, we review the basic idea of the anisotropic diffusion techniques for image smoothing and denoising. In Section IV, we propose the combined hierarchical segmentation and selective smoothing method for images with and without noise. Experimental results are in Section V, and the final section is our conclusion.

II. Segmentation Methods Based on Mumford–Shah Functional

Mumford and Shah proposed and studied the properties of variational problems which are widely applied to the image segmentation problem [15]. The variational principle is essential in this method and its applications. We first present the main idea of the Mumford–Shah segmentation method followed by a

brief review of different forms of the Chan–Vese active contours model in this section.

A. Mumford–Shah Model

The Mumford–Shah method is an energy-based method introduced by Mumford and Shah in 1989 via an energy functional [15]. The basic idea is to find a pair (u, C) for a given image u_0, such that u is a nearly piecewise smooth approximation of u_0, and C is a set of edges between regions within the image. The general form of the Mumford–Shah functional is

$$F(u,C) = \int_{\Omega} |u-u_0|^2 dxdy + \mu \int_{\Omega \setminus C} |\nabla u|^2 dxdy + \nu \cdot \text{length}(C) \quad (1)$$

where μ and ν are nonnegative constants, Ω bounds an open set of R^2 (image domain), the curve $C \subset \Omega$, $\{x, y\} \in \Omega$, and $u_0(x, y)$ is the initial image. $u(x, y)$ is the piecewise smooth function approximation to u_0 with discontinuities *only* along the curve C. To solve the Mumford–Shah problem is to minimize the functional $F(u, C)$ over u and C.

The difficulties in studying $F(u, C)$ are that it involves two unknowns u and C of different natures: u is a function in an N-dimensional space ($N = 2$ in our consideration), while C is an $(N-1)$-dimensional set. The other difficulty is that the functional $F(u, C)$ is not convex, and may have numerous local minima. Therefore, it is not easy to minimize the Mumford–Shah functional (1) in practice. There are some alternative solutions to this problem, such as the elliptic approximation to the weak formulation of the Mumford–Shah functional method [2], the active contours without edges model proposed by Chan and Vese [6], [20], and the curve evolution based approach [19].

B. Chan–Vese Piecewise Smooth Model

From the general form of the Mumford–Shah functional (1), if we consider that there is a closed curve (active contour) C in the image domain Ω, then Ω is partitioned into R and $\overline{R}$ corresponding to the image subdomains inside and outside the curve C, respectively. Minimizing (1) becomes the minimization of the following problem [20], [19]:

$$\begin{aligned} &F(u_1, u_2, C) \\ &= \int_{\text{inside}(C)} |u_1 - u_0|^2 dxdy \\ &\quad + \mu \int_{\text{inside}(C)} |\nabla u_1|^2 dxdy + \int_{\text{outside}(C)} |u_2 - u_0|^2 dxdy \\ &\quad + \mu \int_{\text{outside}(C)} |\nabla u_2|^2 dxdy + \nu \cdot \text{length}(C) \end{aligned} \quad (2)$$

where u_1 and u_2 are the smooth functions approximating the image function u_0 inside and outside the curve, respectively, μ and ν are constants. When we apply the level-set method to this model by replacing the unknown curve $C(t)$ by the level-set function $\phi(x, y, t)$, and consider that $\phi(x, y, t) > 0$ if the point (x, y) is inside C; $\phi(x, y, t) < 0$ if (x, y) is outside C, and $\phi(x, y, t) = 0$ if (x, y) is on C. Minimizing the functional $F(u_1, u_2, \phi)$ with respect to u_1, u_2 and ϕ, we obtain the equations for u_1, u_2 and ϕ as the following:

$$u_1 - u_0 = \mu \nabla^2 u_1 \text{ inside } C, \ \frac{\partial u_1}{\partial \vec{n}} = 0 \text{ on } C \quad (3)$$

$$u_2 - u_0 = \mu \nabla^2 u_2 \text{ outside } C, \ \frac{\partial u_2}{\partial \vec{n}} = 0 \text{ on } C \quad (4)$$

$$\frac{\partial \phi}{\partial t} = \delta(\phi) \left[\nu \nabla \cdot \left(\frac{\nabla \phi}{|\nabla \phi|} \right) - |u_1 - u_0|^2 - \mu |\nabla u_1|^2 + |u_2 - u_0|^2 + \mu |\nabla u_2|^2 \right] \quad (5)$$

where $\delta(\phi)$ is the Dirac δ function. The image functions u_1 and u_2 are obtained by solving the damped Poisson equations (3) and (4) for any given curve C. This is the piecewise smooth case of the Chan–Vese model [20]. Very similar idea has been also developed independently by Tsai *et al.* [19]. The smoothing and denoising effect on the image u_0 comes from solving the PDEs for u_1 and u_2, which are inside and outside the curve, respectively. Therefore, diffusion filtering only happens within different homogeneous regions, but not across the boundaries of such regions. The smoothing approach is very similar to the idea of "anisotropic diffusion" [1], [16], [21]–[23]. Many advantages can be achieved for image segmentation and denoising in this piecewise smooth approach, such as simultaneous segmentation and smoothing of noisy images, detection of triple junctions by using multiple level-set functions [20] (or the approach in [18]), and smoothing the images with complex features [19], [20]. However, in this piecewise smooth approach, there are some disadvantages we would like to address.

i) The capability of denoising is limited because of the damped Poisson equation used for denoising. Furthermore, because the Poisson equations for u_1 and u_2 have the same form and parameters, the same amount of noise will be removed in the homogeneous regions inside and outside the curve C. In some applications, this restriction may limit the flexibility of the method.

ii) Since the method does segmentation and denoising simultaneously, when the image is very noisy, and noise may destroy some parts of the edges, one may not be able to obtain good segmentations of the image.

iii) Computation cost is another problem in this algorithm. There are three PDEs to be solved (3)–(5), and solving the curve evolution (5) involves the other two (3) and (4) in each iteration step. However, only the solutions of (3) and (4) at the final step are the values of the smoothed image. Although many speedup methods have been proposed in [19], it may not work well in practice when the image size is large and the noise ratio is high.

iv) Like the Chan–Vese multiphase piecewise constant approach, if we apply this piecewise smooth method to multiphase segmentation, handling the initial condition is also a problem.

Based on the idea of the Chan–Vese piecewise constant segmentation method [6], [20], we propose a hierarchical approach for multiphase segmentation of an image, and a two-step algorithm for image segmentation and denoising all together. At the

first step, we use the proposed hierarchical segmentation approach to find the boundaries of regions within an image. Then, we apply diffusion filter to each homogeneous region independently but not across the boundaries of such regions. Before we present the proposed method in detail, we review the Chan–Vese piecewise constant method as follows.

C. Piecewise Constant Segmentation Methods

The active contour model proposed by Chan and Vese is a particular case of the Mumford–Shah model. It minimizes the energy functional

$$F(c_i, C) = \sum_i \int_{\Omega_i} (u_0(x,y) - c_i)^2 dxdy + \nu \cdot \text{length}(C) \quad (6)$$

where c_i is the average value of $u_0(x,y)$ in each connected region Ω_i, and $\Omega = \cup_i \Omega_i \cup \text{C}$. ν is a positive constant. Using the Heaviside function $H(\phi)$: $H(\phi) = \begin{cases} 1 & \phi \geq 0 \\ 0 & \phi < 0 \end{cases}$, the energy functional (6) can be represented by the level-set approach with $C(t)$ corresponding to the zero level set $\phi(x,y,t) = 0$. For n-phase image, $m = \log_2 n$ level-set functions $\phi_i(x,y,t)$ are needed.

1) Two–Phase Segmentation ($n = 2$): In this case, $m = 1$, we can use only one level-set function ϕ to represent the two-phase energy [6] as

$$F(c_1, c_2, \phi) = \nu \int_\Omega |\nabla H(\phi)| dxdy + \int_\Omega |u_0 - c_1|^2 H(\phi) dxdy + \int_\Omega |u_0 - c_2|^2 (1 - H(\phi)) dxdy. \quad (7)$$

The curve evolution equation can be obtained by minimizing the energy (7) with respect to ϕ as

$$\frac{\partial \phi}{\partial t} = \delta(\phi) \left[\nu \nabla \cdot \left(\frac{\nabla \phi}{|\nabla \phi|} \right) - (u_0 - c_1)^2 + (u_0 - c_2)^2 \right] \quad (8)$$

where c_1 and c_2 are the average values in regions $\{\phi \geq 0\}$ and $\{\phi < 0\}$, respectively. After solving (8) with the help of c_1, c_2, we obtain the evolution of $C(t)$, which is the boundary between the sets $\{u = c_1\}$ and $\{u = c_2\}$. Therefore, the original image u_0 is segmented into two parts $\{u = c_1\}$ and $\{u = c_2\}$.

2) Four–Phase Segmentation ($n = 4$): In this case, $m = 2$, two level-set functions ϕ_1 and ϕ_2 are needed. Use the same approach as in the two–phase case, we can get the level-set formulation of the four–phase energy functional. The Euler–Lagrange (curve evolution) equations for ϕ_1 and ϕ_2 can be obtained, respectively, by minimizing the energy functional with respect to ϕ_1 and ϕ_2 as the following [20]:

$$\frac{\partial \phi_1}{\partial t} = \delta(\phi_1) \left\{ \nu \nabla \cdot \left(\frac{\nabla \phi_1}{|\nabla \phi_1|} \right) - \left((u_0 - c_{11})^2 - (u_0 - c_{01})^2 \right) H(\phi_2) - \left((u_0 - c_{10})^2 - (u_0 - c_{00})^2 \right) (1 - H(\phi_2)) \right\} \quad (9a)$$

$$\frac{\partial \phi_2}{\partial t} = \delta(\phi_2) \left\{ \nu \nabla \cdot \left(\frac{\nabla \phi_2}{|\nabla \phi_2|} \right) - \left((u_0 - c_{11})^2 - (u_0 - c_{10})^2 \right) H(\phi_1) - \left((u_0 - c_{01})^2 - (u_0 - c_{00})^2 \right) (1 - H(\phi_1)) \right\} \quad (9b)$$

where c_{11}, c_{00}, c_{10}, and c_{01} are the average intensity values in each corresponding region

$$\begin{aligned} c_{11} &= \text{mean}\,(u_0) \text{ in } \{\phi_1 > 0 \text{ and } \phi_2 > 0\} \\ c_{00} &= \text{mean}\,(u_0) \text{ in } \{\phi_1 < 0 \text{ and } \phi_2 < 0\} \\ c_{10} &= \text{mean}\,(u_0) \text{ in } \{\phi_1 > 0 \text{ and } \phi_2 < 0\} \\ c_{01} &= \text{mean}\,(u_0) \text{ in } \{\phi_1 < 0 \text{ and } \phi_2 > 0\}. \end{aligned} \quad (10)$$

Solving the above PDEs (9) for ϕ_1 and ϕ_2 and calculate the average values c_{11}, c_{00}, c_{10}, and c_{01} for each time step, we can obtain the evolution of the curves C_1 and C_2. The moving curves will stop at the boundaries of the objects within the image, hence, we partition the image.

Although this algorithm works well for image segmentation, solving the Euler–Lagrange equations (8) or (9a) and (9b) costs a lot of *CPU* time, especially for real images with large size. There is another method to solve the variational segmentation problem without the need to solve the Euler–Lagrange equation but to calculate the energy directly [18]. The main idea of the direct energy computation algorithm for two-phase segmentation is as follows. 1) Construct an initial partition using an initial curve C ($\phi = 0$) which divides the image into two parts ($\phi > 0$ and $\phi < 0$) and determine two constants c_1 and c_2 which are the averages inside and outside C. 2) Change the sign of ϕ associated with each pixel in the image in a given order and compute the energy, if the energy decreases, then accept the new sign of ϕ and update c_1 and c_2, otherwise ϕ remains unchanged. This method improves the computational speed drastically but can also develop spurious stationary states. In order to eliminate certain spurious stationary states, very recently, a multiscale version of the direct energy computation has been proposed by updating all pixels (instead of only one) in an $n \times m$ neighborhood of the visited pixel [7].

The main disadvantages of the above active contour methods are their computational costs and the initialization problem. For a multiphase (we use the four-phase case as an example) segmentation approach, because of the coupling between the curve evolution equations for ϕ_1 and ϕ_2 [see (9a) and (9b)], the algorithm is slow, and the final results depend on the choice of the initial curves. Although the direct energy computation method speeds up considerably, it is still a problem to obtain "good" initial curves, especially for images with complicated features (see Fig. 1).

In Section IV, we will propose a hierarchical implementation method for multiple phase segmentation in order to overcome the above shortcomings of the Chan–Vese model.

III. Anisotropic Diffusion Method for Image Smoothing

PDE–based, nonlinear anisotropic diffusion techniques are an effective way to smooth and denoise images. The smoothed image can be obtained by the solution $u(x,y)$ of the diffusion equation at a specific time t, with initial conditions $u(x,y,t = 0) = u_0(x,y)$, where $u_0(x,y)$ is the original noisy image. The general formula of a diffusion equation can be written as

$$\begin{aligned} \frac{\partial u(x,y)}{\partial t} &= div\,(D(x,y) \cdot \nabla u(x,y)) \\ u(x,y,t=0) &= u_0(x,y) \end{aligned} \quad (11)$$

where D is the diffusivity. According to the property of the divergence operator, the diffusivity can be a scalar function (or constant) or a tensor (or a tensor-valued function).

The simplest diffusion filter is the linear isotropic diffusion, where the diffusivity is a scalar constant. It smoothes the noise in an image and blurs the edges of objects within it as well. In order to avoid blurring of edges, the nonlinear isotropic diffusion uses a scalar function of the gradient ∇u_σ instead of a constant diffusivity, where u_σ is the convolution of the original image u_0 with a Gaussian filter K_σ that is $u_\sigma \equiv K_\sigma * u_0$ and $D = \mathrm{g}(|\nabla u_\sigma|)$. This diffusivity function satisfies $\mathrm{g}(0) = 1$ and $\mathrm{g}(\mathrm{s}) = 0$ for $\mathrm{s} \to \infty$. Therefore, it behaves as linear diffusion in the interior of a region ($|\nabla u_\sigma| \to 0$) and inhibits diffusion at strong edges ($|\nabla u_\sigma| \to \infty$). The nonlinear isotropic diffusion can avoid blurring of edges, but it cannot eliminate noise at edges.

The anisotropic diffusion technique, first introduced in [16] and further developed in [1] and [5], takes into account both the modulus of the gradient $|\nabla u_\sigma|$ and its direction. Here, D is generally a symmetric positive definite diffusion tensor. It smoothes the image within the homogeneous regions and along the edges depending on the choice of the diffusion tensor, but not across the boundaries. The key point of the anisotropic diffusion approach is how to construct the diffusion tensor D. Weickert proposed two different ways to choose the diffusion tensor D for different diffusion goals, namely the edge-enhancing and coherence-enhancing anisotropic diffusions [21]–[23]. Among the PDE diffusion approaches for image denoising, the anisotropic approach gives the highest performance. The most important advantage of the anisotropic diffusion technique is that it selectively smoothes an image while preserving and relatively enhancing the edges of regions.

In the methods mentioned above, the edge detector is based on the gradient of the convolved image ∇u_σ. In the next section, we will present our proposed method in which the edge detection is not based on the image gradients, and can smooth noisy images anisotropically.

IV. Segmentation Prior to Denoising Method

In this section, we present the hierarchical implementation of multiphase piecewise constant segmentation model, followed by a two-step method for image segmentation and smoothing.

A. Hierarchy Segmentation Method

1) Remarks on Chan–Vese Model: As we mentioned in Section II, the segmentation results obtained by using the Chan–Vese method are dependent on initial conditions. In Fig. 1, we show two experimental examples obtained from the Chan–Vese segmentation algorithm with different initial conditions, we also give the *CPU* times for later comparison by running our C++ programs on Pentium IV 2.40-GHz PC. For both the synthetic image (the first two rows) and the medical image (the last two rows), we get different results of segmentation for different initial curves. For example, when we use four initial circles for the synthetic image (see the far left figure in the first row), we can get the correct segmentations, but we cannot get the correct segmentations when more initial circles are used. For the X-ray hand image, the segmentation results obtained by using different initial circles are different. Chan and Vese suggested that multiple initial conditions should be used [20], but we cannot always get better segmentations by using multiple initial conditions (see the last column of Fig. 1). Therefore, it is a big challenge to find an efficient way to handle the initial conditions in the Chan–Vese multiphase segmentation model.

As mentioned in Section II, the other problem of the Chan–Vese segmentation algorithm is the computation cost. It involves solving multiple coupled PDEs for the curve evolution when multiple level-set functions are used.

2) Weight Parameters in the Two–Phase Segmentation Method: It is well known that using one level-set function in the Chan–Vese model we can segment an image into different regions with two distinct means. If we consider the parameters associated with the "fitting energies" in the energy functional, (7) and (8) can be written as

$$\begin{aligned} F(c_1, c_2, \phi) &= \nu \int_\Omega |\nabla H(\phi)| dxdy + \alpha_1 \int_\Omega |u_0 - c_1|^2 H(\phi) dxdy \\ &\quad + \alpha_2 \int_\Omega |u_0 - c_2|^2 (1 - H(\phi)) dxdy \end{aligned} \tag{12}$$

$$\frac{\partial \phi}{\partial t} = \delta(\phi) \left[\nu \nabla \cdot \left(\frac{\nabla \phi}{|\nabla \phi|} \right) - \alpha_1 (u_0 - c_1)^2 + \alpha_2 (u_0 - c_2)^2 \right] \tag{13}$$

where α_1 and α_2 are parameters associated with the energy inside and outside the segmenting curve, respectively. Actually, the energy inside (or outside) the curve is the statistical measurement of an image within the region inside (or outside) the curve. Parameters α_1 and α_2 behave as weight factors in the statistical measurement. If $\alpha_1 > \alpha_2$, the energy functional inside the curve is more important than the one outside the curve; therefore, we can get more detailed segmentations inside the curve, and vice versa. Fig. 2 shows the experimental results for two given images. The first row in Fig. 2 presents (a) a synthetic image with one initial curve, (b) the segmented image by choosing $\alpha_1 = \alpha_2 = 1$, and (c) the segmented image by choosing $\alpha_1 = 2$, $\alpha_2 = 1$. Those results show that when we use the same weight factors ($\alpha_1 = \alpha_2$) in both regions, we can only detect two objects out of three. If we want to emphasize the region for $\phi > 0$ by choosing the weight factors $\alpha_1 > \alpha_2$, we can detect the three objects with the same initial curve. Fig. 2(d) shows an original MRI knee stir image with one initial curve, and (e)–(i) are the segmented results of the MRI image obtained by fixing $\alpha_2 = 1$, and varying α_1. It can be seen that we can get more details of the segmented results by increasing the weight parameter α_1 to a certain limit. When the parameter α_1 becomes too large, some features are lost [see Fig. 2(i)]. Using different parameters in different regions allows us to obtain more detailed segmentations in specific regions. From our experimental results, the best choice of α_1/α_2 is $\alpha_1/\alpha_2 \approx \sigma_I^2/\sigma_{II}^2$, where $\sigma_I^2 = \int_{\Omega_I} (u_I - c_I)^2 dxdy / \int_{\Omega_I} dxdy$ and similarly for σ_{II}^2. Subscripts I and II denote the *segmented* regions with $\phi > 0$ and $\phi < 0$, respectively. This ratio is usually between 1 and 5. From (13), we see that when the parameter ν becomes larger (e.g., $\nu \geq \sigma^2$), the first term on the RHS becomes more significant and the method becomes less sensitive to the setting of

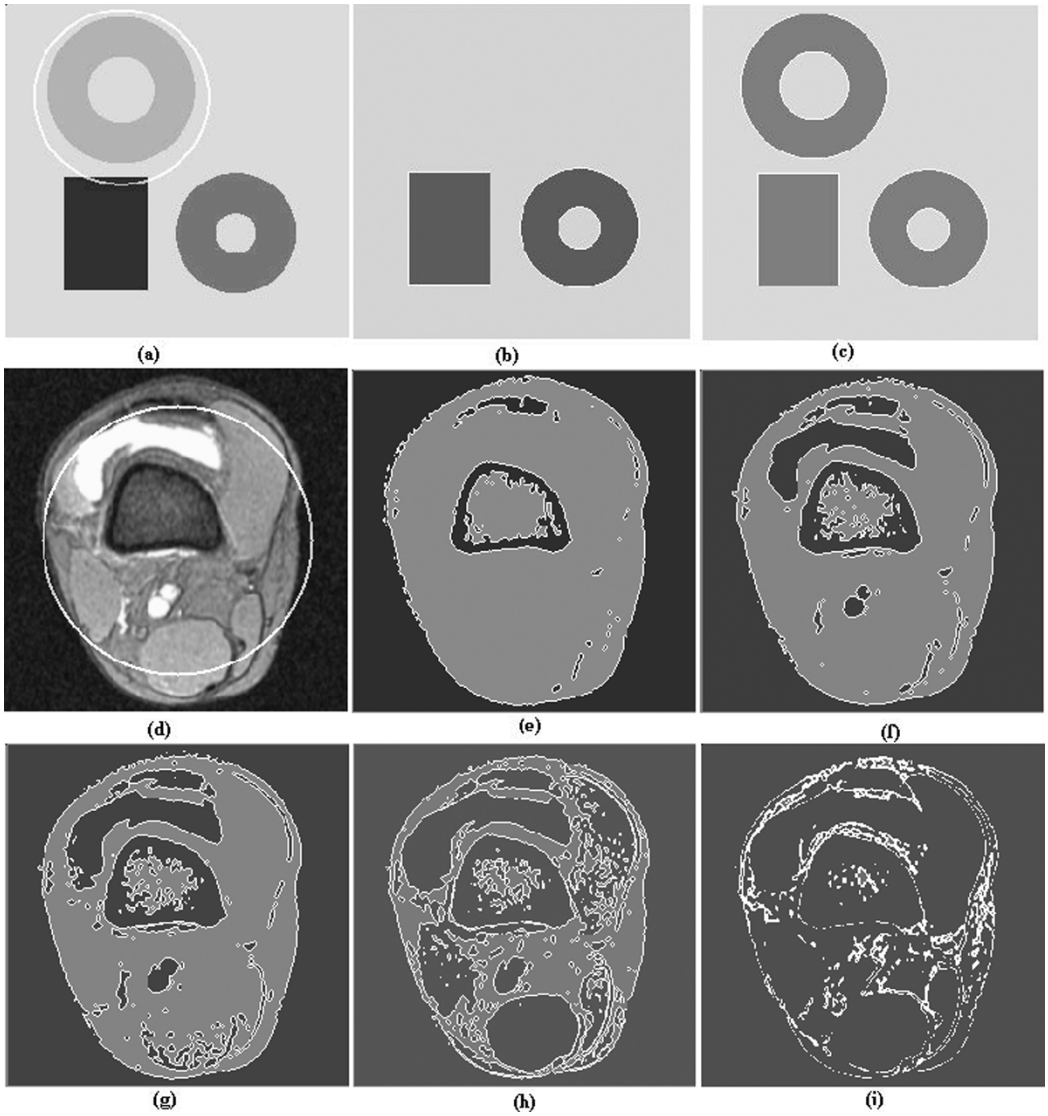

Fig. 2. Two–phase segmentation results with different parameters α_1 and α_2, $\nu = 1$. (a) Original synthetic image with one initial curve. (b) $\alpha_1 = 1$ and $\alpha_2 = 1$. (c) $\alpha_1 = 2$ and $\alpha_2 = 1$. (d) Original MRI knee stir image with one initial curve. (e)–(i) $\alpha_2 = 1$. (e) $\alpha_1 = 1$. (f) $\alpha_1 = 3$. (g) $\alpha_1 = 5$. (h) $\alpha_1 = 10$. (i) $\alpha_1 = 50$.

α_1/α_2. Because this ratio can only be obtained after the segmentation has been completed, it is not very useful in practice, and, moreover, we cannot completely segment an image with multiple distinct means by just changing this ratio. Therefore, we do not recommend this approach of using one level-set function and changing the α_1/α_2 ratio. In order to obtain detailed segmentations of an image and better performance of the algorithm, we propose a hierarchical approach of multiphase segmentation which is faster than the Chan–Vese algorithm. Furthermore, the initial conditions are much easier to handle in our method.

3) Hierarchical Multiphase Segmentation Method: Using a piecewise smooth representation of the Mumford–Shah model, Tsai *et al.* have proposed a hierarchical approach for multiphase segmentation [19]. In this approach, they first apply the piecewise smooth algorithm to the original image. Then the same algorithm is applied to the particular subregions which require additional segmentation. This method has many disadvantages because only one level-set function is used, and it cannot detect in advance which parts require additional segmentations. We now present our hierarchical approach for multiphase piecewise constant segmentation model. This approach works in multiple segmentation stages. At the *first* stage, we apply the Chan–Vese piecewise constant segmentation model with one level-set function ϕ_1 to a given image. At the end of the *first* segmentation stage, we get *two* resulting subregions. It should be noted that each subregion may contain many isolated parts. Then the second stage starts by applying the same model with another level-set function ϕ_2 to each of the subregions independently. After the *second* segmentation, we get *four* resulting sub-subregions. Next, we apply the same model with the third level-set function ϕ_3 to each of those sub-subregions, and so on. Our experimental results show that most gray level real images require two level-set functions. The four-color theorem can be used to justify the partition by using two level-set functions [20], but, in practice, a third level-set function may be needed for images with very complicated features, because of the local minima problem.

We now illustrate our multiphase hierarchical approach through the case of the four–phase (two level-set functions) segmentation. Like the Chan–Vese model, there are two

evolution curves C_1 and C_2, which are represented by the corresponding level-set functions ϕ_1 and ϕ_2. At the *first* segmentation stage, the evolution of the curve C_1 is governed by the motion equation of the level-set function ϕ_1

$$\frac{\partial \phi_1}{\partial t} = \delta(\phi_1)\left[\nu_0 \nabla \cdot \left(\frac{\nabla \phi_1}{|\nabla \phi_1|}\right) - \alpha_1 (u_0 - c^{\mathrm{I}})^2 + \alpha_2 (u_0 - c^{\mathrm{II}})^2\right] \tag{14}$$

where c^{I} is the average of u_0 inside C_1 ($\phi_1 > 0$) and c^{II} is the average of u_0 outside C_1 ($\phi_1 < 0$). At the end of the *first* segmentation stage, we obtain two subregions, defined by $\{\phi_1 > 0\}$, and $\{\phi_1 < 0\}$. At the *second* segmentation stage, we apply the curve evolution PDE of C_2 (represented by ϕ_2) to these two subregions separately; therefore, for subregion *I* $\{\phi_1 > 0\}$, we have the curve evolution PDE

$$\frac{\partial \phi_2}{\partial t} = \delta(\phi_2)\left[\nu_I \nabla \cdot \left(\frac{\nabla \phi_2}{|\nabla \phi_2|}\right) - \alpha_1 (u_0 - c_1^{\mathrm{I}})^2 + \alpha_2 (u_0 - c_2^{\mathrm{I}})^2\right] \tag{15a}$$

where c_1^{I} is the average of u_0 in subregion *I* and also inside the curve C_2 ($\phi_1 > 0$, $\phi_2 > 0$) and c_2^{I} is the average of u_0 in subregion *I* but outside the curve C_2 ($\phi_1 > 0$, $\phi_2 < 0$).

For subregion *II* $\{\phi_1 < 0\}$, the curve evolution PDE is

$$\frac{\partial \phi_2}{\partial t} = \delta(\phi_2)\left[\nu_{II} \nabla \cdot \left(\frac{\nabla \phi_2}{|\nabla \phi_2|}\right) - \alpha_1 (u_0 - c_1^{\mathrm{II}})^2 + \alpha_2 (u_0 - c_2^{\mathrm{II}})^2\right] \tag{15b}$$

where c_1^{II} is the average of u_0 in subregion *II* and also inside C_2 ($\phi_1 < 0, \phi_2 > 0$) and c_2^{II} is the average of u_0 in subregion *II* but outside C_2 ($\phi_1 < 0$, $\phi_2 < 0$). After the second segmentation, we obtain the final four segments of a given image.

Unlike the Chan–Vese multiphase active contour model [20], in our hierarchical method instead of applying the level-set functions ϕ_1 and ϕ_2 simultaneously to an image, we apply ϕ_1 and ϕ_2 one after another. Thus, the motion equations of ϕ_1 (14) and ϕ_2 (15) are completely decoupled. The decoupling of the curve evolution PDEs we use here is similar to the operator splitting or fractional steps techniques developed by Yanenko [24] for the numerical solutions of coupled PDEs. Each equation alone behaves the same as the curve evolution PDE in the simple two–phase (one level-set function) segmentation model; therefore, it is fast. The decoupling of the motion PDEs also allows us to choose different values of the parameters ν_0, ν_I, and ν_{II} for different stages. Since the first term in the Mumford–Shah model (1) is actually the least square fitting of energy; therefore, we can choose these parameters in the following way: The variance of a region Ω in the image u can be calculated by $\sigma^2 = \int_\Omega (u - \overline{u})^2 dxdy / \int_\Omega dxdy$, where $\overline{u}$ is the mean value of u in Ω. At the first stage, one can choose the parameter $\nu_0 = \beta\sigma^2$, where β is a constant between 0 and 1.5. The smaller the value of ν_0 the finer the segmentations and the faster the algorithm. If we do not want to detect smaller objects like points created by noise, then ν_0 should be larger [6]. At the end of the first stage, we have two regions *I* $\{\phi > 0\}$ and *II* $\{\phi < 0\}$, we can calculate the variances σ_I^2 and σ_{II}^2 in these two regions. If the variance σ_I^2 is larger than σ_{II}^2 then region *I* needs more detailed segmentations than region *II*. Based on this fact, we can set parameters $\nu_I = \sigma_{II}^2$ and $\nu_{II} = \sigma_I^2$. Our observations are as follows: For images with small amounts of noise, we can choose $\beta \leq 0.5$ and $\nu_I = \nu_{II} = \min(\sigma_I^2, \sigma_{II}^2)$; for images with large amount of noise, we have to set $\beta = 1 \sim 1.5$ and $\nu_I = \sigma_{II}^2$, $\nu_{II} = \sigma_I^2$. The *direct energy computation approach* can be implemented in exactly the same way.

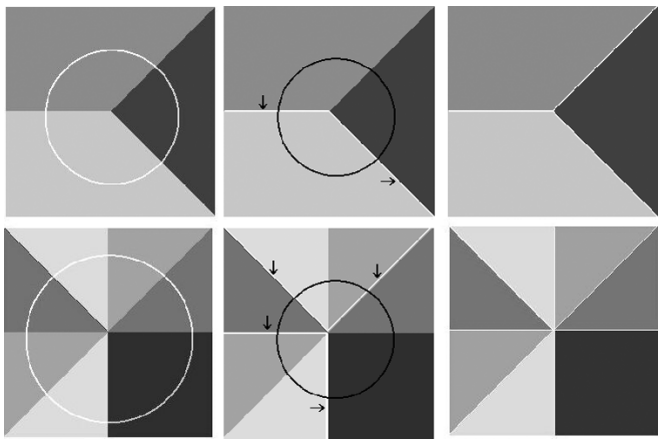

Fig. 3. Four–phase segmentation using our hierarchical method. Left column: Original synthetic image with the initial curve of ϕ_1. Middle column: Results after the first segmentation (see the white lines indicated by arrows) with the initial curve of ϕ_2. Right column: Final segmented images. ($\nu = 0$, CPU = 1.7 s, image size 256 × 256 for both images).

We show how the proposed hierarchical segmentation method works through an example as shown in Fig. 3. The left column contains two original synthetic images with the initial curve of ϕ_1 (white). The middle column contains the segmented images at the end of the first stage with the initial curve of ϕ_2 (black) superimposed. The right column contains the final segmentations of the two given images which show that the triple and multiple junctions within the image are detected. From Fig. 3, we can see that the first segmentation is like a coarse segmentation of an image, while the second does more detailed segmentation. Actually, this hierarchical method starts with a crude segmentation and refines the segmentation down to the different subregions in order to capture finer and finer details in a given image.

The initial condition is easy to handle in our hierarchical method because curve evolution equations are decoupled. At each segmentation stage, only one curve evolution equation represented by a single level-set function is involved. Therefore, just one level-set function needs to be initialized. In one level-set evolution case, we can get sufficient result by using one single initial curve [6], [18]. In our implementation, we use a single initial curve for the level-set function ϕ_1 at the first segmentation stage to get a crude segmentation. Although we also use a single curve to initialize ϕ_2 for the second segmentation, the actual initial condition of ϕ_2 is multiple curves because of the presence of the final stage of ϕ_1. The edges obtained by the first segmentation (white curves in the middle column of Fig. 3) together with the initial curve of ϕ_2 (the black curve in the middle column of Fig. 3) make the actual initial condition of ϕ_2.

In this hierarchical approach, edges obtained from the first stage together with the initial curve of the second level-set function automatically construct the real initial condition of the curve evolution equation at the second stage. Edges obtained at the end of second stage together with the initial curve of the third level-set function construct the actual initial condition of the curve evolution equation at the third stage, and so on. We can get sufficient segmentations by using single initial curve for

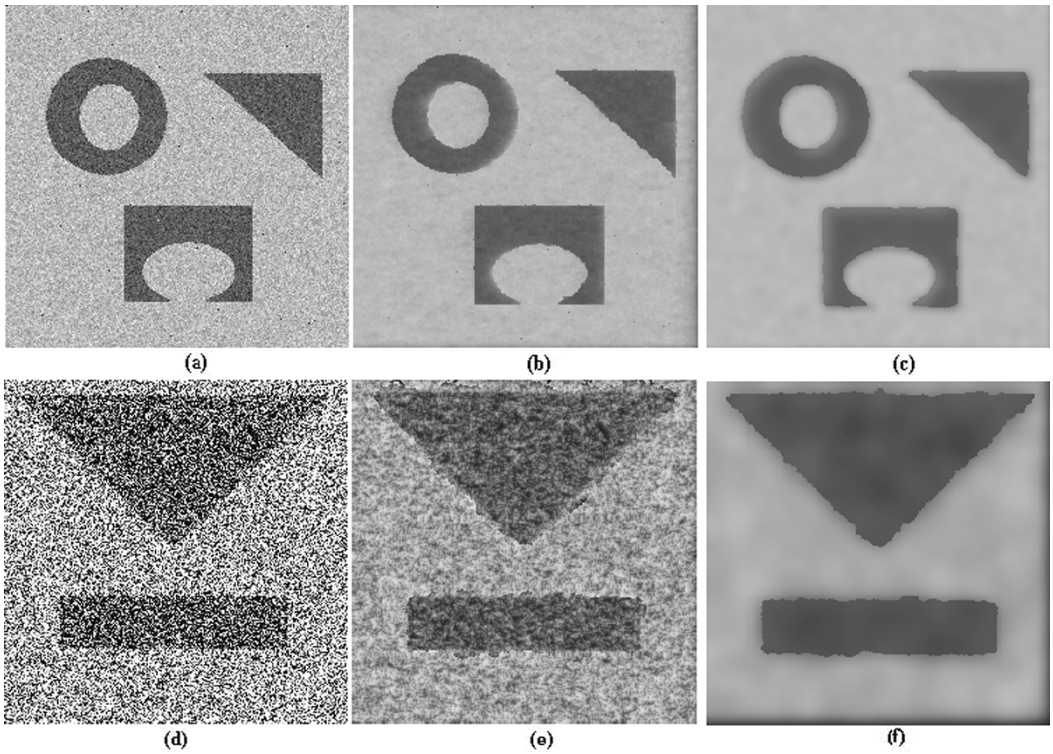

Fig. 4. Segmentation and smoothing of noisy synthetic images using different approaches. (a), (d) Original noisy images. (b), (e) Reconstruction by Chan–Vese piecewise smooth approach. (b) $\nu = 1.5\sigma^2 = 2714$, CPU $= 103.5$ s, error $= 0.59$. (e) $\nu = 11086$, CPU $= 181.1$ s, error $= 0.50$. (c), (f) Reconstruction by our proposed approach. (c) $\nu = 1.5\sigma^2 = 2714$, CPU $= 7.3$ s, error $= 0.51$. (f) $\nu = 1.5\sigma^2 = 16\,629$, CPU $= 25.0$ s, error $= 0.42$. Image size: 256×256.

each individual level-set function, as long as the initial curve contains the regions (objects) we want to segment.

As we already mentioned in Section II, the piecewise constant segmentation method represents each segment of an image by a constant. The more general Mumford–Shah segmentation method is the piecewise smooth representation of an image, which has been addressed in [20], [19]. In order to get better performance for denoising and segmentation of an image, we propose a new two-step segmentation and smoothing method as follows.

B. Two–Step Segmentation and Smoothing Method

The basic idea of the segmentation and denoising algorithm is to obtain different subregions within a given image by using our hierarchical segmentation method first, then use each subregion of the original noisy image as the initial condition (input) of the diffusion equation for denoising. Therefore, we can smooth each subregion separately but not across the edges between the subregions. This algorithm works in the following steps.

i) Apply our hierarchical segmentation method to the noisy image u and partition the image into different regions.
ii) The result of segmentation in step *i*) (i.e., ϕ values) is applied to the original image u. Let u^{I} be the original image in region for $\{\phi \geq 0\}$, and u^{II} be the original image in region for $\{\phi < 0\}$. We then apply the diffusion filter to the different regions of u independently. In order to solve the diffusion equations in different regions properly, we need to extend u^{I} to the region $\{\phi < 0\}$ and u^{II} to the region $\{\phi \geq 0\}$. For instance, to extend u^{I} to the region $\{\phi < 0\}$, we can use the average constant approximation of u in region $\{\phi < 0\}$. Other extension method can be found in **[20]**. Attention must be paid to the boundaries between the regions. We can use the Neumann boundary conditions $\partial u^{\mathrm{I}}/\partial \vec{n} = 0$ or $\partial u^{\mathrm{II}}/\partial \vec{n} = 0$ ($\vec{n}$ is the normal of the curve C) when we extend u^{I} or u^{II} across the edges between regions. Therefore, the diffusion does not cross the boundaries of different regions.

Our proposed method is fast since detecting the boundary of the regions only requires updating the average values inside and outside the active contours. This method is more flexible since we can choose different diffusion parameters (or different smoothing methods) for different subregions depending on the applications. So, it can process very noisy images without difficulties. This may be useful in applications such as medical image segmentation and smoothing. The previous piecewise smooth algorithm [20], [19] does not perform well for very noisy images.

We use the signal-to-noise ratio *SNR* to estimate the quality (or the amount of noise) of the image u with respect to a reference image (usually, the "clear" image) u_0. It is defined by

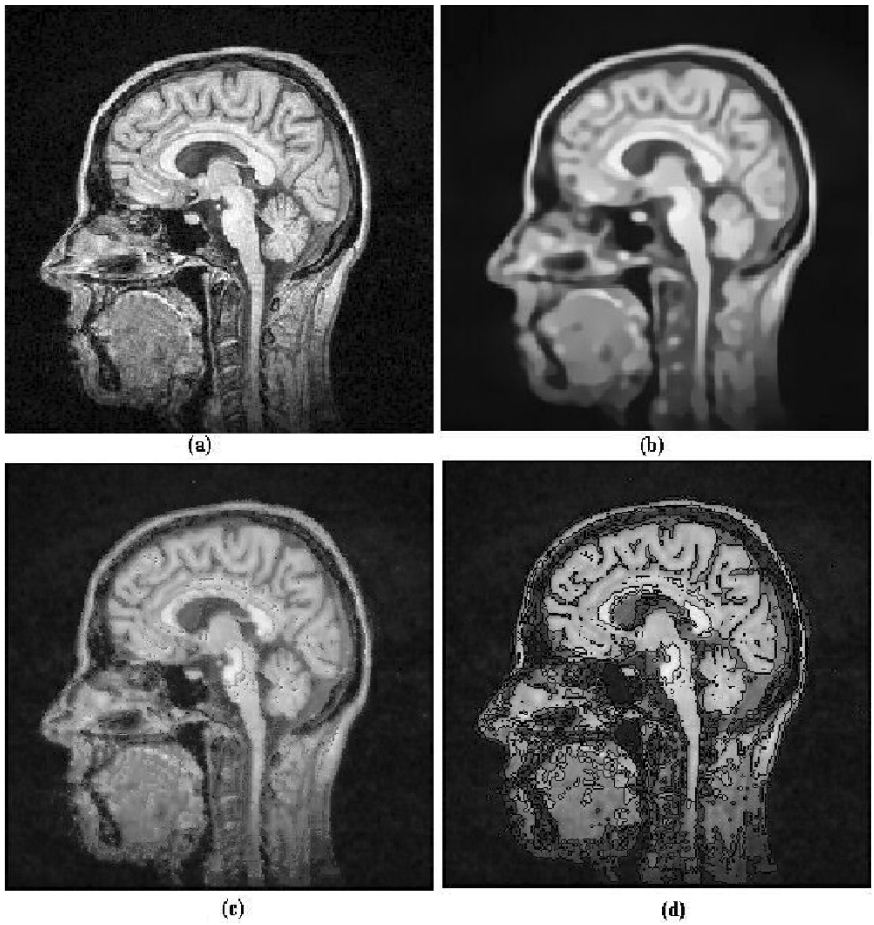

Fig. 5. Smooth and edge-enhancement of a medical image. (a) Slice of an MRI image. (b) After anisotropic edge-enhancing diffusion filtering by Weickert [23]. (c) Final result after segmentation and smoothing of the image. (d) After segmentation and smoothing, segmenting curves are superimposed on the image.

SNR $= 10\log_{10}\left(||u||^2/||u_0-u||^2\right)$, where $||\cdot||$ denotes the Euclidean norm.

In Fig. 4, for comparison, we show the segmentation and denoising results obtained from piecewise smooth algorithm developed by [20], [19] and our proposed method. We also compare the *CPU* time (in seconds) and the error ratio for these two algorithms. The error ratio is defined by $error = ||u_0-u_d||^2/||u_0-u_n||^2$, where u_0 is "clear" image, u_n is noisy image [e.g., (a) and (d)] and u_d is denoised image. For an image with small amount of noise (a) (SNR $= 16.29$ dB), the smoothing image (b) obtained by the piecewise smooth algorithm [20], [19] is acceptable. If the image is very noisy (d) (SNR $= 2.69$ dB), the smoothed image (e) obtained by the Chan–Vese piecewise smooth approach is not as good as desired. Our proposed two-step method is better than the Chan–Vese method both in performance (see the error ratios) and in efficiency (see the *CPU* times). The proposed algorithm first segments the given image into subregions, then the diffusion equation is applied within each subregion but not across the edges; therefore, the edges are preserved. This is very similar to the smoothing process in anisotropic diffusion [1], [21], [22].

As we already mentioned, the proposed segmentation and smoothing method which adapts itself in an anisotropic way to the evolving image is well suited for smoothing noise while simultaneously preserving important features such as edges. This characteristic may be important in medical image processing. In Fig. 5, we show an example where a denoising and edge enhancing process has been applied to an MRI brain image. The result obtained by using our proposed method is shown in (c). Compared with the result using the edge enhancing anisotropic diffusion filter developed by Weickert [23] which is shown in (b), the proposed method gives better edge enhancing results. We attribute this to the fact that the edge detection is not based on the gradient of the image in our method. Fig. 5(d) shows the segmenting curves superimposed on the resulting image.

V. Experimental Results

We present the segmentation results of the images without noise, followed by the segmentation and smoothing results of the proposed algorithm for noisy images.

A. Segmentation Results

Since the energy functional which is minimized in the Mumford–Shah model is not convex; the segmentation algorithm may not converge to the global minimum for some given initial conditions. As we have shown in Fig. 1, it is difficult to handle the initial conditions in the Chan–Vese multiphase active contour model [20]. In the following examples, we show that it is easy

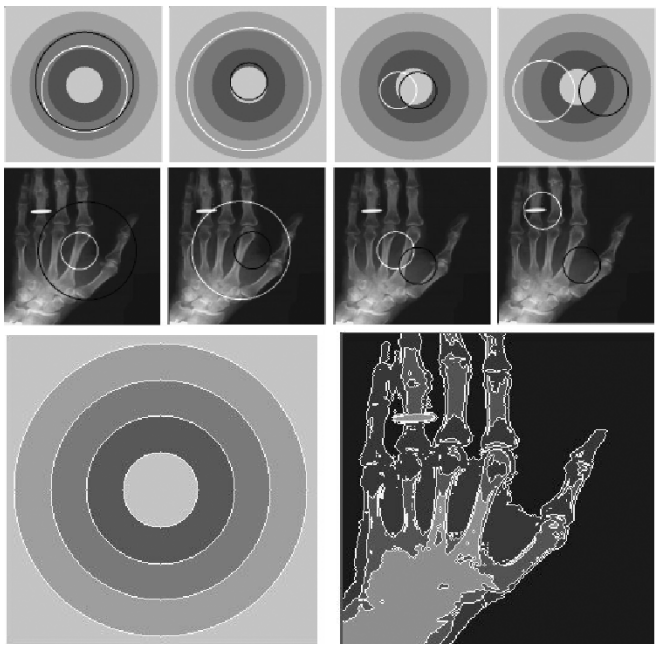

Fig. 6. Our segmentation results with different initial conditions. First and second rows show different initial conditions (white curves for ϕ_1, while black curves for ϕ_2) for images as shown in Fig. 1. The last row shows the segmentation results using different initial curves. Synthetic image: $\nu_0 = \nu_I = \nu_{II} = 1$, CPU $= 1.5$ s. X-ray hand image: $\nu_0 = \nu_I = \nu_{II} = 1$, CPU $= 21.4$ s. Image size: 256×256.

to deal with the initial conditions in our hierarchical segmentation method.

In Fig. 6, we present the segmentation results for a synthetic image and a real X-ray hand image with different initial conditions. These are the same images used in Fig. 1. The detected edges are superimposed on top of the resulting images. In each case, all those different initial curves give the same segmentation results. We also tested on other images and obtained the same segmentations for different initial conditions. Our observation is that, as long as the initial curve contains (or partially contains) the regions we want to detect, we can obtain the same segmentation results regardless of the positions and sizes of the initial curves.

In the next example, we demonstrate how the proposed hierarchical segmentation method works for medical images. The segmentation results of different medical images with multiple distinct regions are shown in Fig. 7. The left column contains the original images which are MRI chest (contains small amount of noise) and ultrasound (contains large amount of noise) from top to bottom, and the initial curves of ϕ_1 and ϕ_2 superimposed on them. The middle column contains the final results using our hierarchical segmentation. The right column contains the same final results with the segmenting curves superimposed. With this simple choice of initial curves, we can obtain good segmentation results.

B. Segmentation and Denoising Results

We now demonstrate how the proposed algorithm works for the noisy images. Both synthetic images and real medical images with additive Gaussian noise are used in our experiments.

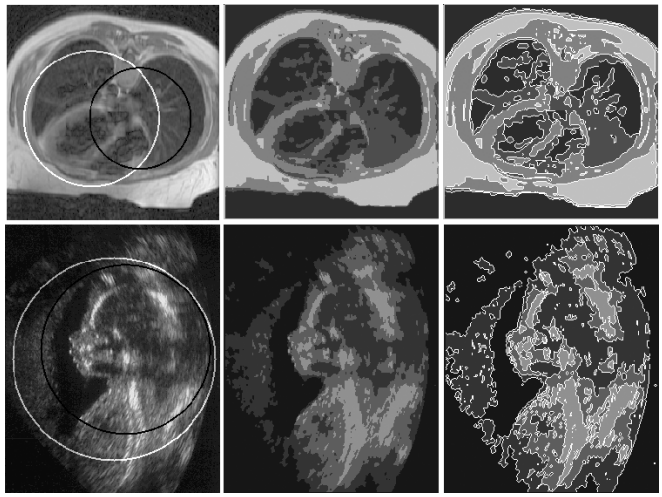

Fig. 7. Segmentation of medical images. Left column: Original images with initial curves, white curves for ϕ_1 while black curves for ϕ_2. Middle column: Final results using our hierarchical segmentation method. Right column: Final segmentations and the segmenting curves superimposed. MRI chest: $\nu_0 = 1$, $\nu_I = \nu_{II} = \min(\sigma_I^2, \sigma_{II}^2) = 610$, CPU $= 34.8$ s, image size: 256×256. Ultrasound image: $\nu_0 = 0.5\sigma^2 = 996, \nu_I = \sigma_{II}^2 = 1368, \nu_{II} = \sigma_I^2 = 447$, CPU $= 79.5$ s, image size: 256×320.

The segmentation and denoising result of a noisy synthetic image with multiple distinct means is shown in Fig. 8. In this case, in order to obtain better performance, two level-set functions are needed. For comparison we present the denoising result by using one level-set function (after the first stage) in Fig. 8(b). We get two regions of the image at that stage, one region is the black triangle while the white rectangle and the background are assigned to the other region. Then we apply our diffusion procedure that behaves as an isotropic diffusion in each homogenous region. Since the triangle and the background belong to different regions, the edges of the triangle are preserved as expected, but the edges of the rectangle are blurred because they belong to the same region of the background, and the diffusion in this region is isotropic. Fig. 8(c) shows the result by using two level-set functions. Since two different objects and the background are in three different regions and diffusion filtering is applied to each region separately; therefore, all edges of the objects are preserved. Because the objects within the image are big, we can simply choose $\nu_0 = \nu_I = \nu_{II} = \sigma^2$.

Since medical image segmentation and denoising is an important problem in image processing, in the next experimental example, we show the performance of our hierarchical multiphase segmentation method in real medical images. In Fig. 9, we present an MRI chest image with additive Gaussian noise and an ultrasound image with "natural noise" from top to bottom in the left column, and the denoised results by using our two-step smoothing method. The segmentation and reconstruction of the two images are shown in the middle column. The right column contains the final resulting images with the segmenting curves superimposed on them. It should be noted that the proposed algorithm removes noise very well and preserves and enhances the edges of different regions.

In the last example, we demonstrate how the combined hierarchical segmentation and selective smoothing method works

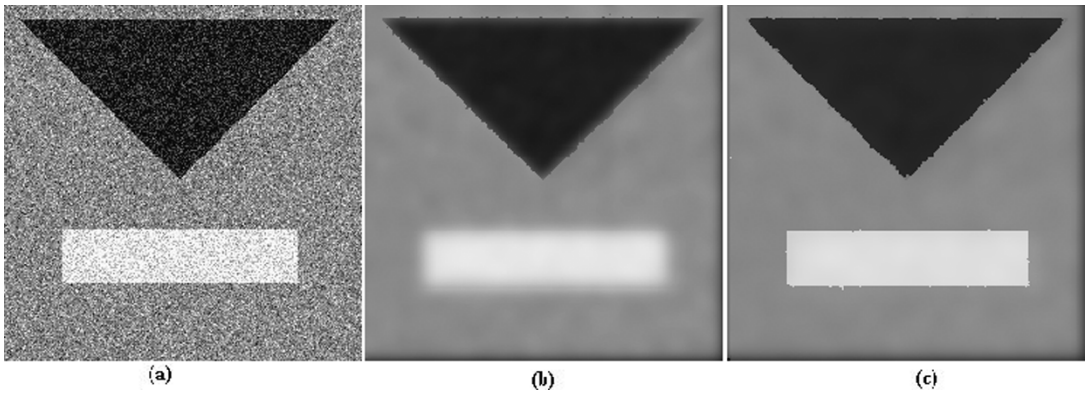

Fig. 8. Segmentation and smoothing of a very noisy synthetic image. (a) Image with Gaussian noise (SNR $= 10.49$ dB). (b) Reconstructed image using the proposed method with one level-set function. (c) Reconstructed image using the proposed method with two level-set functions ($\nu_0 = \sigma^2 = 4302$, CPU $= 67.3$ s, SNR $= 13.8$ dB).

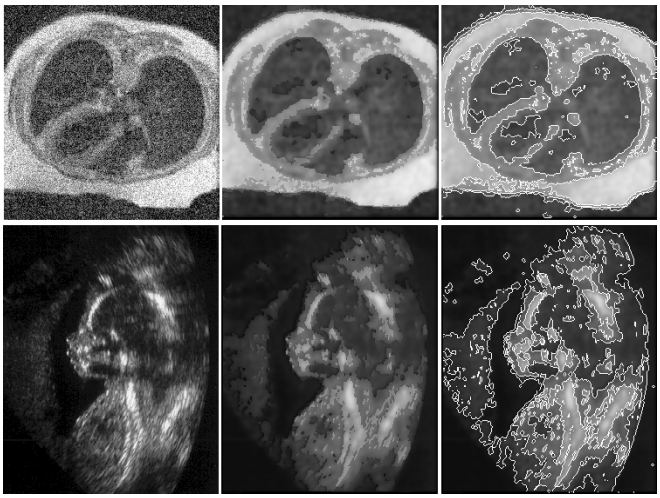

Fig. 9. Segmentation and smoothing of noisy medical images. Left column: (Top, SNR $= 11.06$) Original chest image with Gaussian noise and (bottom) original ultrasound image with natural noise. Middle column: Final segmented and reconstructed image based on the proposed method with two level-set functions. Right column: Segmenting curves are superimposed on final reconstructed images. Noisy MRI chest: $\nu_0 = \sigma^2 = 4448, \nu_I = \sigma_{II}^2 = 2584$, $\nu_{II} = \sigma_I^2 = 1901$, CPU $= 43.5$ s. Size: 256×256), and the parameters are same as in Fig. 7 for the noisy ultrasound image (CPU $= 82.9$ s).

for a real MRI knee stir image. The original image is shown in Fig. 10(a) with initial curves for ϕ_1 and ϕ_2, and (e) shows the final reconstruction of the image and the segmenting curves superimposed on it. It can be seen from this resulting image some details within the image, such as the white stripe in the upper part and two small round white matters in the lower part which cannot be detected by the Chan–Vese method or our method with $\alpha_1/\alpha_2 = 1$. In order to get more details within the region of interest, as discussed in Fig. 2, we can choose different values of the weight parameters α_1 and α_2 in the *first* segmentation stage. It is easy to specify the parameters with a single initial curve at the *first* stage. For example, for the initial (white) curve as shown in Fig. 10(a), we can get more details inside the curve by choosing $\alpha_1 > \alpha_2$. In (b) and (c), we use piecewise constant representations to show the final gray segmentation maps corresponding to the final reconstruction results of (e) and (f), respectively.

These figures demonstrate that our segmentation and smoothing method provides better details in different regions, relatively enhances the edges between regions, and highlights the regions of interest.

VI. Conclusion

In this paper, we have proposed and implemented a new image segmentation and smoothing algorithm based on the Chan–Vese active contour model and PDE–based diffusion techniques. The level-set method is employed in our numerical implementation. This algorithm works in two steps, first segmenting the noisy image by using hierarchical piecewise constant segmentation method, then using PDE-based diffusion method to smooth and denoise each segmented region of the original image separately but not across the boundaries.

Because of the coupling of different curve evolution PDEs associated with different level-set functions in the Chan–Vese multiphase segmentation algorithm, the initialization of the level-set functions becomes a difficult problem. The proposed hierarchical approach decouples the curve evolution PDEs makes the initialization problem easy to handle and also speeds up the algorithm. In Table I, we show the *CPU* times and errors (for noisy images) of the Chan–Vese method and our proposed method, our method is more efficient and has better performance for noisy images than the Chan–Vese method.

Compared with the previous simultaneous segmentation and smoothing methods [20], [19], the proposed method is more efficient and flexible. First, we separate the segmentation and smoothing processes and use hierarchical piecewise constant segmentation algorithm in the segmentation process. Therefore, it improves the computational speed drastically and makes the initial condition easy to handle. Second, the proposed method allows us to apply different smoothing algorithms in different regions in an image; therefore, it is very convenient when the applications need to highlight some special regions in an image. In this paper, isotropic diffusion was used for denoising. However, other denoising approaches, such as wavelet thresholding [3], can also be employed. The wavelet–based denoising algorithms are very different in technique from the PDE denoising methods, but they are quite close in spirit and in experimental

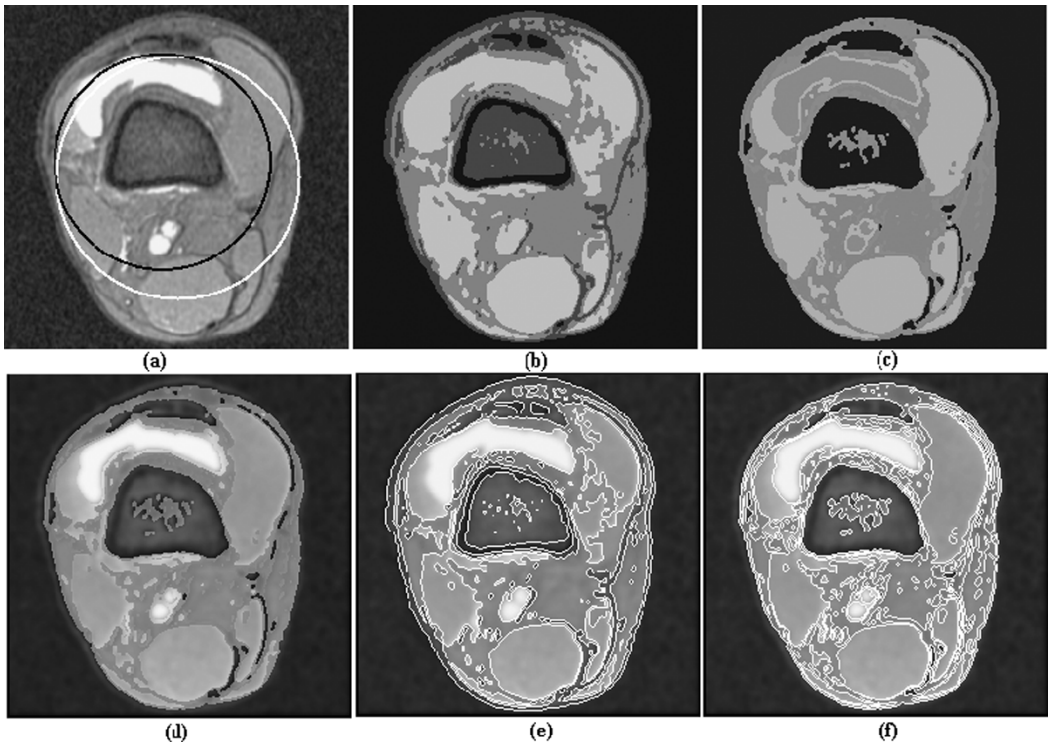

Fig. 10. Segmentation and smoothing of real MRI knee stir image. (a) Original image with initial curves; white curve for ϕ_1 and black curve for ϕ_2. (b) and (c) Final segmented images represent in piecewise constants with different ratio of α_1/α_2. (b) $\alpha_1/\alpha_2 = 1$, (CPU $= 30.5$ s). (c) $\alpha_1/\alpha_2 = 3$, (CPU $= 49.3$ s). (d) Final reconstructed image ($\alpha_1/\alpha_2 = 3$, CPU $= 49.5$ s). (e) and (f) Final segmented and reconstructed image with segmenting curves. (e) $\alpha_1/\alpha_2 = 1$, (CPU $= 31.2$ s). (f) $\alpha_1/\alpha_2 = 3$, (CPU $= 49.5$ s). Parameters: $\nu_0 = 1$, $\nu_I = \sigma_{II}^2 = 816$, $\nu_{II} = \sigma_I^2 = 1096$.

TABLE I
CPU TIMES (IN SECONDS) OF THE CHAN–VESE METHOD AND OUR PROPOSED METHOD

	Synthetic image	x-ray hand image	Noisy image Fig.4 (a)	Noisy image Fig.4 (d)
Chan-Vese method	**28.2 Fig. 1**	**60.1 Fig. 1**	**103.5 (error: 0.59) Fig. 4 (b)**	**181.1 (error: 0.50) Fig. 4 (e)**
Our proposed method	**1.5 Fig. 6**	**21.4 Fig. 6**	**7.3 (error: 0.51) Fig. 4 (c)**	**25.0 (error: 0.42) Fig. 4 (f)**

results [14]. Like anisotropic diffusion methods, the proposed algorithm only smoothes the image within the homogeneous regions but not across the boundaries; thus, edges are preserved during the denoising process.

The proposed method can process very noisy images well. Our experimental results show that, for a very noisy image [see Fig. 4(d), for instance], we can still detect the objects and preserve the boundaries of the objects within the image when removing noise. Actually, this model can perform active contours, denoising, segmentation and edge detection in a unified way.

Regularization by convolving a Gaussian filter with the original noisy image is widely used in PDE–based denoising methods [5], [21]. Throughout this paper, we do not apply the regularization to the noisy images; however, for very noisy image, preprocessing, the image by regularization is recommended.

ACKNOWLEDGMENT

The authors would like to thank the reviewers for carefully reading the manuscript, which lead to further improvement of the paper.

REFERENCES

[1] L. Alvarez, P. L. Lions, and J. M. Morel, "Image selective smoothing and edge detection by nonlinear diffusion II," *SIAM J. Numer. Anal.*, vol. 29, no. 3, pp. 845–866, 1992.

[2] G. Aubert and P. Kornprobst, *Mathematical Problems in Image Processing: Partial Differential Equations and the Calculus of Variations*. New York: Springer, 2002, vol. 147.

[3] T. D. Bui and G. Y. Chen, "Translation invariant denoising using multiwavelets," *IEEE Trans. Signal Process.*, vol. 46, no. 12, pp. 3414–3420, Dec. 1998.

[4] V. Caselles, R. Kimmel, and G. Sapiro, "Geodesic active contours," *Int. J. Comput. Vis.*, vol. 22, pp. 61–79, 1997.

[5] F. Catte, P. L. Lions, J. M. Morel, and T. Coll, "Image selective smoothing and edge detection by nonlinear diffusion," *SIAM J. Numer. Anal.*, vol. 29, no. 1, pp. 182–193, 1992.

[6] T. F. Chan and L. A. Vese, "Active contours without edges," *IEEE Trans. Image Process.*, vol. 10, no. 2, pp. 266–277, Feb. 2001.

[7] T. F. Chan and S. Esedoglu, "A multiscale algorithm for Mumford–Shah image segmentation," Univ. California, Los Angeles, CAM, 03-77, 2003.

[8] D. Freedman and T. Zhang, "Active contours for tracking distributions," *IEEE Trans. Image Process.*, vol. 13, no. 4, pp. 518–526, Apr. 2004.

[9] M. Kass, A. Witkin, and D. Terzopoulos, "Snakes: Active contour models," *Int. J. Comput. Vis.*, vol. 1, pp. 321–331, 1988.

[10] B. B. Kimia and K. Siddiqi, "Geometric heat equation and nonlinear diffusion of shapes and images," *Comput. Vis. Image Understand.*, vol. 64, no. 3, pp. 305–322, 1996.

[11] R. Malladi and J. A. Sethian, "Image processing via level set curvature flow," in *Proc. Nat. Acad. Sci. USA*, vol. 92, Jul. 1995, pp. 7046–7050.

[12] ——, "Image processing: Flows under Min/Max curvature and mean curvature," *Graph. Models Image Process.*, vol. 58, no. 2, pp. 127–141, 1996.
[13] A. Mansouri and J. Konrad, "Multiple motion segmentation with level sets," *IEEE Trans. Image Process.*, vol. 12, no. 2, pp. 266–277, Feb. 2003.
[14] P. Mrazek, J. Weickert, and G. Steidl, "Correspondences between wavelet shrinkage and nonlinear diffusion," in *Scale-Space 2003*, L. D. Griffin and M. Lillholm, Eds. New York: Springer, 2003, vol. 2695, Lecture Notes in Computer Science, pp. 101–116.
[15] D. Mumford and J. Shah, "Optimal approximation by piecewise smooth functions and associated variational problems," *Comm. Pure Appl. Math*, vol. 42, pp. 577–685, 1989.
[16] P. Perona and J. Malik, "Scale-space and edge detection using anisotropic diffusion," *IEEE Trans. Pattern Anal. Mach. Intell.*, vol. 12, no. 5, pp. 629–639, May 1990.
[17] J. A. Sethian, *Level Set Methods and Fast Marching Methods*. Cambridge, MA: Cambridge Univ. Press, 1999.
[18] B. Song and T. F. Chan, "A fast algorithm for level set based optimization," Univ. California, Los Angeles, CAM, 02-68, 2002.
[19] A. Tsai, A. Yezzi, and A. S. Willsky, "Curve evolution implementation of the Mumford–Shah functional for image segmentation, denoising, interpolation, and magnification," *IEEE Tran. Image Process.*, vol. 10, no. 8, pp. 1169–1186, Aug. 2001.
[20] L. Vese and T. F. Chan, "A multiphase level set framework for image segmentation using the Mumford and Shah model," *Int. J. Comput. Vis.*, vol. 50, no. 3, pp. 271–293, 2002.
[21] J. Weickert, *Anisotropic Diffusion in Image Processing*. Stuttgart, Germany: Taeubner, 1998.
[22] ——, "Theoretical foundations of anisotropic diffusion in image processing," *Comput. Suppl.*, vol. 11, pp. 221–236, 1996.
[23] J. Weickert and C. Schnörr, "PDE-based preprocessing of medical images," *Künstliche Intell.*, no. 3, pp. 5–10, 2000.
[24] N. N. Yanenko, *The Method of Fractional Steps*. New York: Springer-Verlag, 1971.
[25] A. Yezzi, L. Zollei, and T. Kapur, "A variational framework for integrating segmentation and registration through active contours," *Med. Image Anal.*, vol. 7, pp. 171–185, 2003.
[26] S. Zhu and A. Yuille, "Region competition: Unifying snakes, region growing, and Bayes/MDL for multiband image segmentation," *IEEE Trans. Pattern Anal. Mach. Intell.*, vol. 18, no. 9, pp. 884–900, Sep. 1996.

Song Gao received the M.S. degree in physics from the Central China Normal University, Wuhan, China, in 1990, the M.S. degree in computer science from Concordia University, Montreal, QC, Canada, and the Ph.D. degree in physics from Fudan University, Shanghai, China, in 1995.

He was a Postdoctoral Fellow in the Department of Physics, McGill University, Montreal, in 1996. He held the Humboldt Research Fellowship at the University of Frankfurt, Frankfurt, Germany, from 1997 to 1999. He is currently a Postdoctoral Fellow with the MD Anderson Cancer Center, University of Texas, Houston. His areas of research interest are image processing and applications to medicine.

Tien D. Bui (M'92) received the B.S. degree in electrical engineering from the University of Ottawa, Ottawa, ON, Canada, in 1968, the M.S. degree in aeronautical engineering from Carleton University, Ottawa, in 1969, and the Ph.D. degree in physics from York University, Toronto, ON, in 1971.

He was with the Department of Mechanical Engineering, McGill University, Montreal, QC, Canada, from 1971 to 1974. He joined the Department of Computer Science, Concordia University, Montreal, in 1974, was promoted to Full Professor in 1984, and became Chair of the Department from 1985 to 1990. In June 1992, he was appointed to Associate Vice-Rector Research at Concordia University and remained in this position until 1996. He has served on various governing bodies of the Concordia University, including its Senate. During the period from 1992 to 1996, he served as a member of the Boards of Directors/Governors of many research centers and institutes in Quebec, including the Centre de Recherche Informatique de Montreal, Inc. (CRIM), the Institut de Recherche sur les Populations (IREP), the Institut des Sciences Mathematiques (ISM), and GRIAO (a consortium of many research labs on VLSI in Quebec universities). He was also a member of the Committee of Vice-Rectors Research in Quebec (CREPUQ). He is an Associate Editor of the *International Journal of Wavelets, Multiresolution and Information Processing* and the *Transactions of the Society for Modeling and Simulation*.

Dr. Bui was a member of the organizing committees/program committees of many international conferences, including the Second and Third International Conferences on Wavelet Analysis and Its Applications in 2001 and 2002, respectively, in Hong Kong and Beijing, China, respectively, and the ICWAA '03, and the International Conference on Pattern Recognition (ICPR'02) in Quebec City, QC. He has served as a member of grant selection committees and as an External Reviewer for federal and provincial granting agencies, including the Quebec Government MESS Selection Committee of international exchange programs. He has published more than 120 papers in different areas in scientific journals and conference proceedings. He is coauthor of the book *Computer Transformation of Digital Images and Patterns* (Singapore: World Scientific, 1989). His current interests are in wavelet transforms and PDEs with applications to machine intelligence, pattern recognition, and image and video processing.